ISBN: 978-3-95450-184-7 doi:10.18429/JACoW-IPAC2018-TUPAL040

ION BEAM STUDIES IN THE FRIB FRONT END*

T. Yoshimoto†, K. Fukushima, S. M. Lidia, T. Maruta, P. N. Ostroumov, E. Pozdeyev, H. Ren
Facility for Rare Isotope Beams, Michigan State University, MI 48824, East Lansing, USA

Abstract

The commissioning of the FRIB Front End (FE) with 12 keV/u argon beam started in the summer of 2017. Beam profile monitors were used to evaluate RMS Twiss parameters in various locations along the beam line. Beam dynamics in the LEBT was simulated using full 3D model of beam optics elements in the tracking codes. We found a good consistency between measured and simulated data. A beam image viewer was used to measure the beam density distribution in the real space. A hollow beam structure was observed in the Ar^{9+} beam with the current of ~20 μA. Extensive beam dynamics studies with 3D tracking code suggest that the hollow density distribution can be generated by space charge effects of the multi-component, multi-charge state ion beams just after the ECR ion source. This paper reports studies of a mechanism that can produce a hollow beam structure.

INTRODUCTION

The main mission of FRIB project is to deliver 400 kW uranium beam to the target for rare isotope production. To achieve this ambitious goal, multiple charge state beams will be simultaneously accelerated through the FRIB superconducting linac. The beam commissioning of the FE has been performed with Ar^{9+} [1, 2]. Currently, the room temperature Artemis-B ion source is used in the FE. The second, high-power ion source similar to VENUS [3], will be installed later.

The layout of the Artemis-B line is shown in Fig. 1. All ion beams including Ar^{9+} are being continuously extracted by applying 15 kV, focused by an solenoid and accelerated through a DC acceleration column up to 12 keV/u. There is another solenoid upstream of the 90° combined focusing magnet. After the bending, survived contaminant beams can be scraped with a horizontal and vertical movable collimating system. Then, the beam of interest can be characterized by a screen image and Allison scanners installed between two electrostatic triplets.

HOLLOW BEAM DISTRIBUTION

At the initial beam commissioning stage, we observed a beam with a hollow beam structure on the viewer screen, which is installed in the charge selection area after the first magnetic dipole.

Typical screen images for 5 μA and 27 μA Ar^{9+} beams with the ion source drain current of 31 μA and 168 μA, respectively, are shown in Fig. 2. A hollow structure was observed in the 27 μA case. This comparison suggests that this phenomenon is most likely caused by the beam space charge upstream of the bending magnet.

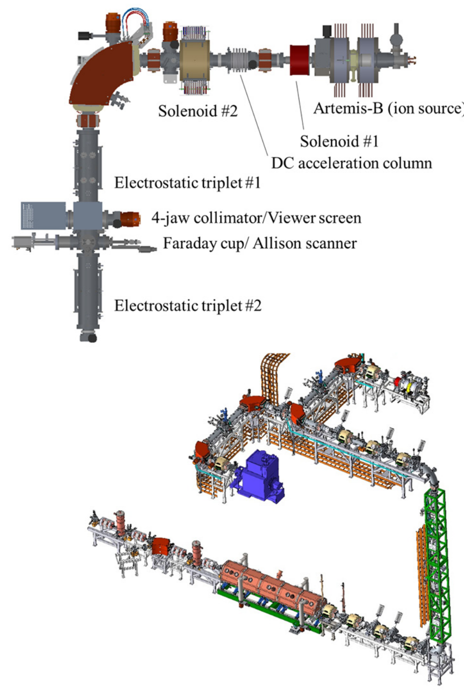

Figure 1: Layout of the FRIB Artemis-B ion source line (top) and FRIB Frontend line (bottom).

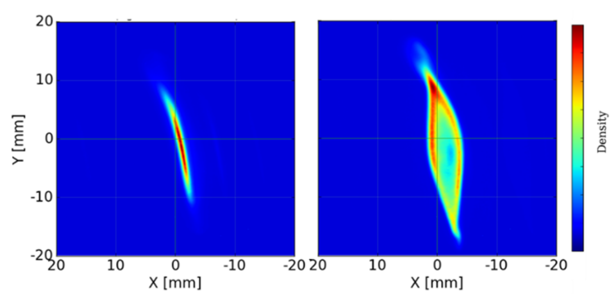

Figure 2: Screen images of Ar^{9+} beam with the current of 5 μA (left), and 27 μA (right) on each normalized color scale.

In the 27 μA case, the maximum brightness ratio of the local minimum point inside the hollow structure to the peak intensity is 32 %. As an additional proof of the hollow structure, the beam distributions of the downstream wire profile monitors are shown in Fig. 3. Some of the horizontal and vertical beam profiles have two peaks. In a simple explanation, two beam cores are rotated through the LEBT on the 2D phase spaces, *x-x′* and *y-y′* planes.

3D PARTICLE TRACKING

It is difficult to estimate initial beam Twiss parameters at the ECR exit by backtracking ions from the location of charge selector due to the space charge effects caused by

*Work supported by the U.S. Department of Energy Office of Science under Cooperative Agreement DE-SC0000661 and the National Science Foundation under Cooperative Agreement PHY-1102511, the State of Michigan and Michigan State University.

† yoshimot@frib.msu.edu.

ISBN: 978-3-95450-184-7 doi:10.18429/JACoW-IPAC2018-TUPAL040

multi-charge and multi-component ion beam transport upstream of the bending magnet. The established procedure is as follows:

1. The Ar^{9+} beam current is set less than 10 μA to minimize space charge effects prior to the separation of ion species and charge states in the bending magnet.
2. Beam images were taken on the viewer for different setpoints of the electrostatic quadrupoles to determine the horizontal and vertical rms beam sizes and coupling terms in the σ-matrix of the beam as shown in Fig. 4. With series of datasets, we can determine the 4D beam σ-matrix including coupling terms of $<xy>$, $<xy'>$, $<x'y>$, and $<x'y'>$ just before the charge selection dipole magnet using the envelope code, FLAME [4].
3. With the particle tracking code, TRACK3D [5], which can implement full 3D grid maps for electric and magnetic components, one can find the 4D beam σ-matrix at the beam extraction point by fitting to the measured σ-matrix in the location of the viewer as shown in Fig. 5. In this optimization, the space charge effect is not taken into account due to negligible contribution. We assumed Gaussian beam distributions in the 4D phase space. After that, the same initial normalized rms emittances, and Twiss parameters, and coupling terms of $<xy>$, $<xy'>$, $<x'y>$, and $<x'y'>$ are applied to ten charge states of argon beam, Ar^{3+} -Ar^{12+} as shown in Fig. 6. It implies the assumption that initial beam Twiss parameters of the beam extracted from the ECR ion source do not strongly depend on the beam current due to neutralized plasma condition inside of the ion source chamber.

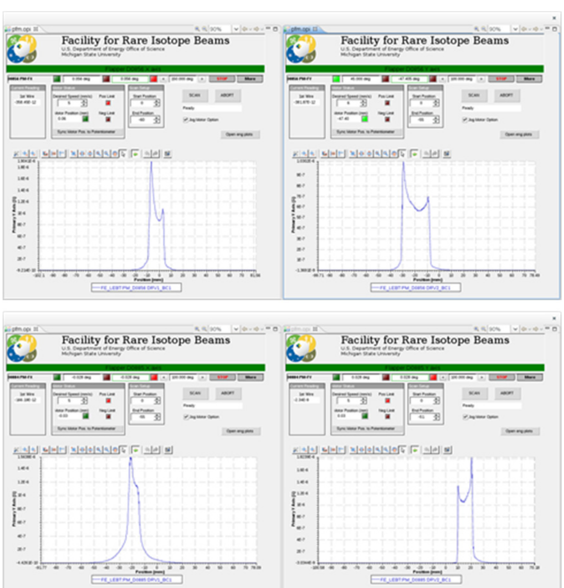

Figure 3: Horizontal (left) and vertical (right) beam distributions measured by wire profile monitors in the vertical LEBT line. Positions of the wire scanners are 17 m (top) and 20 m (bottom) from the ion source (see Ref. [1, 2]).

The normalized horizontal and vertical rms emittances calculated with a least square optimization method from the measured data, ε_x and ε_y, are 0.087 and 0.055 π·mm·mrad with the Twiss parameters, α_x, α_y, β_x, β_y of 0.48, 0.59, 0.11 m/rad, 0.08 m/rad just after the 15 kV extraction electrode of the ion source.

With above initial beam property and space charge contribution of multi-charge-state ion beams which current distribution is summarized in Table 1, we were able to reproduce beam images at the viewer location for the 5 μA and 27 μA beams. A hollow structure for the higher current is clearly seen from Fig. 7. The simulated beam images are very similar to those shown in Fig. 2. The comparison of beam parameters is summarized in Table 2.

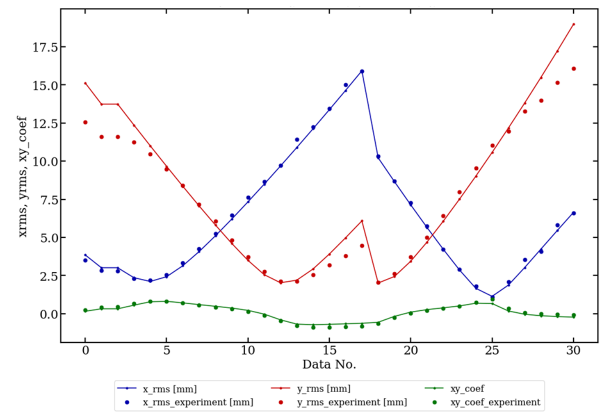

Figure 4: Electrostatic quad scanning result. Blue, red, and green dots denote horizontal and vertical beam size, $\sqrt{<x^2>}$, $\sqrt{<y^2>}$ in mm, and xy coupling coefficient is $<xy>/\sqrt{<x^2>}\sqrt{<y^2>}$. Solid lines correspond to the fitting results.

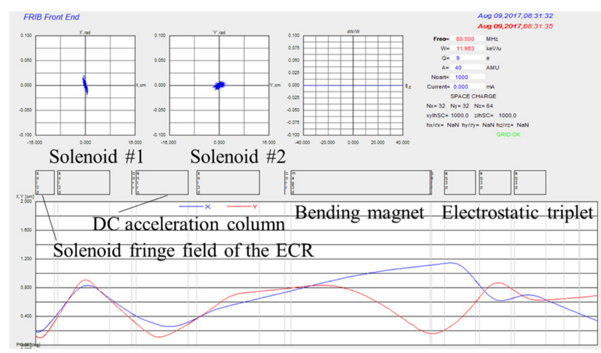

Figure 5: Ar^{9+} beam horizontal and vertical envelopes (red and blue lines) with the reconstructed beam σ-matrix just after the extraction electrode without space charge effects in TRACK simulation.

Each component in the multi-charge state beam has a different focal point due to different magnetic focusing strength as shown in Fig. 8. The horizontal and vertical phase space plots in Fig. 8 describe ten different charge states of argon beam in different color dots. If the multi-charge beam is overfocused, it creates stronger space charge effects in the waste. To avoid a formation of small-size beam waists, the position of the ECR puller was adjusted to change the beam optics upstream of the bending magnet.

ISBN: 978-3-95450-184-7 doi:10.18429/JACoW-IPAC2018-TUPAL040

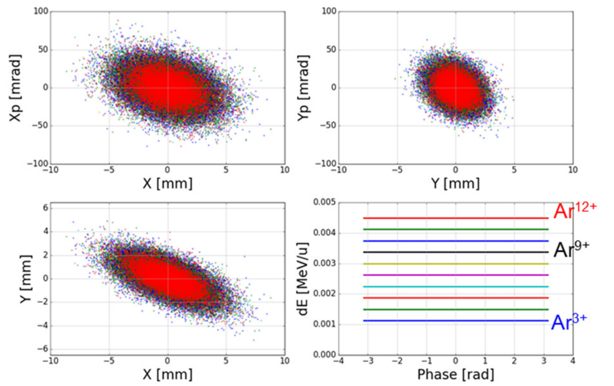

Figure 6: The initial beam distribution in the 6D phase space at the ECR extraction point. Each color indicates different charge state of argon.

Table 1: Typical Argon Beam Current Distribution for Different Charge State

Ion species	Current, μA
$^{40}Ar^{12+}$	1.2
$^{40}Ar^{11+}$	4.6
$^{40}Ar^{10+}$	13.5
$^{40}Ar^{9+}$	27.0
$^{40}Ar^{8+}$	42.0
$^{40}Ar^{7+}$	22.2
$^{40}Ar^{6+}$	18.3
$^{40}Ar^{5+}$	16.2
$^{40}Ar^{4+}$	11.4
$^{40}Ar^{3+}$	11.3

Table 2: Beam Parameter Comparison for 5μA and 27 μA Ar^{9+} Beam Current

Parameters	Simulation	Measurement
5 μA		
x_{rms}, mm	1.9	1.7
y_{rms}, mm	5.8	5.5
xy coupling	0.76	0.76
27 μA		
x_{rms}, mm	2.3	1.9
y_{rm}s, mm	6.5	7.2
xy coupling	0.58	0.61

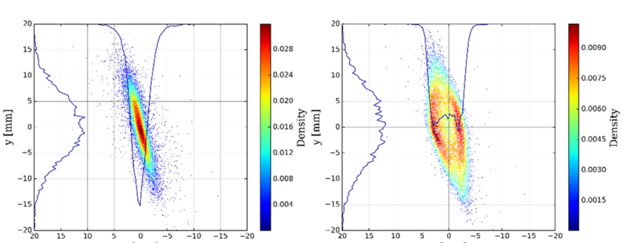

Figure 7: Simulated Ar^{9+} beam distributions with a current of 5 μA (left), and 27 μA (right) at the viewer location.

CONCLUSION

The hollow beam structure observed in the beam image measurements was well reproduced in the numerical simulation. The results suggest that the multi-charge-state beam with different focal points for each charge state can cause a hollow beam structure especially in the optics setting with small-size envelope waists. To avoid this unfavorable situation, we have developed a new optics setting by modifying the ECR puller position.

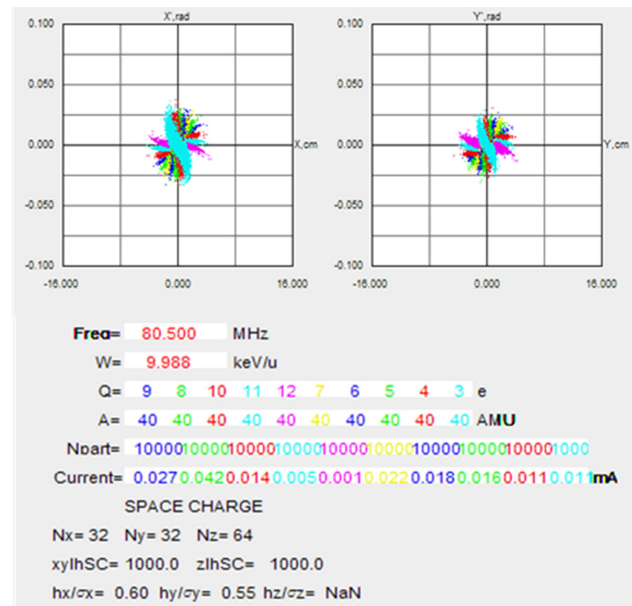

Figure 8: The transverse phase space distribution for Ar^{12+} to Ar^{3+} just before the first magnetic dipole in TRACK simulation.

ACKNOWLEDGEMENTS

The authors would like to thank G. Machicoane, J. Stenson, and S. Renteria for their support for our beam study, and A. Plastun, Q. Zhao, and J. Wong for intensive discussions.

REFERENCES

[1] E. Pozdeyev *et al.*, "FRIB Front End Construction and Commissioning", presented at IPAC'18, Vancouver, Canada, Apr.-May 2018, paper MOZGBF1, this conference.

[2] P. N. Ostroumov *et al.*, "Accelerator Physics Advances at FRIB", presented at IPAC'18, Vancouver, Canada, Apr.-May 2018, paper THYGBF4, this conference.

[3] J. Y. Benitez *et al.*, "Recent progress on the superconducting ion source VENUS", *Rev. Sci. Instrum.*, vol. 83, 02A311, 2012.

[4] Z. He *et al*, "Linear envelope model for multicharge state linac", *Phys. Rev. ST Accel. Beams*, vol. 17, 034001, 2014.

[5] TRACK, `https://www.phy.anl.gov/atlas/TRACK/Trackv39/tv39_index.html`